Tetragonal-orthorhombic phase coexistence under magnetic fields in $BaFe_2As_2$ and $Sr(Fe_{1-x}Co_x)_2As_2$: evidence of magnetically driven structural transition

U. F. Kaneko,[1,2] M. M. Piva,[3] C. B. R. Jesus*,[3] M. E. Saleta†,[3] P. G. Pagliuso,[3] R. R. Urbano,[3] and E. Granado[3]

[1] *"Gleb Wataghin" Institute of Physics, University of Campinas (UNICAMP), Campinas, São Paulo 13083-859, Brazil*
[2] *Brazilian Synchrotron Light Laboratory (LNLS), Brazilian Center for Research in Energy and Materials (CNPEM), Campinas, São Paulo 13083-970, Brazil*
[3] *"Gleb Wataghin" Institute of Physics, University of Campinas - UNICAMP, Campinas, São Paulo 13083-859, Brazil*

Synchrotron x-ray diffraction experiments were performed on $BaFe_2As_2$ and $Sr(Fe_{1-x}Co_x)_2As_2$ single crystals as a function of temperature and applied magnetic field along the tetragonal $[1\bar{1}0]$ direction, complemented by electrical resistivity and specific heat experiments. For a $BaFe_2As_2$ crystal with spin-density-wave antiferromagnetic ordering temperature $T_{AF} = 132.5$ K and onset of the orthorhombic phase at $T_o = 137$ K, the magnetic field favors the growth of tetragonal domains that compete with orthorhombic ones for $T \gtrsim T_{AF}$. For a $Sr(Fe_{1-x}Co_x)_2As_2$ crystal with more separated transitions ($T_{AF} = 132$ K and $T_o = 152$ K), the crystal structure also shows significant field-dependence in a narrow temperature interval close to T_{AF}. These results favor magnetism as the driver of the structural and nematic transitions in 122 Fe pnictides.

I. INTRODUCTION

The high critical temperatures observed in Fe-based superconductors (FeSCs) and similarities with the phase diagrams of cuprates and heavy-fermion superconductors triggered a strong interest on these materials[1–5]. An important ingredient to the physics of the FeSCs is the anisotropic in-plane resistivity that normally occur in detwinned crystals below the onset temperature of the orthorhombic phase T_o . Such anisotropy is associated with an electronic nematic phase[6,7], and the corresponding fluctuations may play an important role in the superconducting pairing mechanism[8]. The spin, charge/orbital and lattice configurations and/or fluctuations are coupled to each other in the FeSCs, and the identification of the primary order parameter associated with the nematic transition is not straightforward[3,4]. The similar values of T_o and the antiferromagnetic (AFM) ordering temperature T_{AF} in some materials, most notably AFe_2As_2 (A=Ca, Sr, and Ba)[9–13], points to a close relationship between electronic nematicity, crystal structure and magnetism. This perception is reinforced by the fact that the stripe AFM phase breaks the four-fold symmetry of the lattice, providing a natural link to an orthorhombic distortion and electronic transport anisotropy. On the other hand, another parent compound of the FeSCs, LaFeAsO, shows significantly separated magnetic and structural transition temperatures ($T_{AF} = 140$ K and $T_o \sim 155$ K)[7,15–17]. An increased separation between T_{AF} and T_o is also seen in AFe_2As_2 under chemical substitution or pressure, such as in the $BaFe_{2-x}Co_xAs_2$ series[12,18,19]. Finally, FeSe at ambient pressure shows a nematic transition at $T_o = 90$ K[20] without presenting long-range magnetic order down to the lowest temperatures. This fact motivated a proposal that the nematic transition may be driven by charge/orbital degrees of freedom rather than magnetism[21,22]. Despite the significant separation between T_o and T_{AF} in LaFeAsO, recent Raman scattering experiments supported the magnetic scenario for the nematic transition of this compound[23]. Even for FeSe the magnetic scenario for nematicity may still apply, since the magnetic correlation length does not have to be large at T_o[24]. It is worth mentioning that the orbital differentiation of the Fe $3d$ orbital may play an important role in both scenarios, since the weight of their occupation at the Fermi level is intertwinned with electronic anisotropy and anisotropic magnetic coupling in this material[25].

A new dimension on the coupling between crystal structure and magnetic ordering in Fe pnictides may be gained by investigating the sensitivity of the crystal structure to an external magnetic field. In this work, we report the magnetic field and temperature dependence of the crystal lattice in $BaFe_2As_2$ (BFA) and $Sr(Fe_{1-x}Co_x)_2As_2$ (SFCA) single crystals with similar $T_{AF} \sim 132$ K, but different T_o ($T_o = 137$ and 152 K for BFA and SFCA, respectively). Our results demonstrate that, while the equilibrium between the competing tetragonal and orthorhombic phases experience important changes with temperature near the bulk transitions at T_{AF} and T_o identified by specific heat and resistivity measurements, such equilibrium is appreciably influenced by the external magnetic field only at $T \gtrsim T_{AF}$. Our results indicate that the competing tetragonal/orthorhombic phase equilibrium is tuned by a magnetic dipolar coupling even in the non-magnetic phase, favoring the scenario where magnetism rather than orbital ordering is the primary driver of the structural transition in Fe pnictides.

*Permanent address: Programa de Pós-Graduação em Física, Campus Prof. José Aluísio de Campos, UFS, São Cristóvão, Sergipe 49100-000, Brazil

†Permanent address: CONICET - Centro Atómico Bariloche, CNEA, San Carlos de Bariloche, Rio Negro, Argentina.

II. EXPERIMENTAL DETAILS

$BaFe_2As_2$ (BFA) and $Sr(Fe_{1-x}Co_x)_2As_2$ (SFCA) single crystals were synthesized by the In flux method as described elsewhere[13,14]. The samples are in the form of thin plates with dimensions of $1-2$ mm in the ab plane. The Co-content of the SFCA sample is $x = 0.24(3)$, determined using an energy dispersive spectroscopy (EDS) microprobe. The EDS measurements were performed in one side of the crystal, and the reported Co content is an average of the values obtained at several spots of the crystal surface. Such relatively large value of x might seem at first sight inconsistent with the presence of magnetic ordering and structural phase transitions (see below), considering previous studies in this family[27–29]. However, it is well known that the detailed phase diagrams of Fe pnictides may depend sensibly on the detailed growth procedure[13]. Specific heat measurements were performed in a small mass calorimeter using the thermal relaxation technique. The in-plane electrical resistivity was measured using a four-contact configuration and low-frequency ac-resistance bridge. Both experiments were performed on cooling in a commercial multi-functional equipment. Synchrotron x-ray diffraction experiments were performed at the XDS beamline of the Brazilian Synchrotron Laboratory (LNLS)[26] in separate beamtime periods for each sample. A sagittal focusing double Si(111) crystal monochromator and Rh-coated vertically collimating and focusing mirrors were employed as optical elements of the beamline. The selected wavelengths were $\lambda = 1.1269$ Å for the measurements on BFA and $\lambda = 0.6196$ Å for SFCA, calibrated with a powder diffraction scan of a LaB_6 NIST standard. The beam dimensions were $\sim 0.2(V)\times2(H)$ mm^2 at the sample position. A 10 K closed cycle He cryostat holding the crystals was mounted in the Eulerian cradle of a low-magnetic 6+2 circle diffractometer. A cryogen-free 6 T high-T_c superconducting magnet with an angular aperture of 120° for the diffracted beam was also attached to the diffractometer. A problem with one of the current sources of the magnet limited the maximum field at 3.5 T for SFCA. The experiments were performed in the vertical scattering plane and the employed geometry provided access to (hhl) reciprocal space positions (tetragonal cell). The magnetic field was applied horizontally, along the tetragonal $[1\bar{1}0]$ direction. The diffracted beam was detected using a setup attached to the 2θ arm of the diffractometer, including a scattering slit close to the magnet, a vertical resolution slit of 1 mm placed at ~ 1 m from the sample and a high-throughput LaBr scintillator point detector. The lattice parameters of the studied crystals are $a = 3.9469(3)$ Å and $c = 12.986(1)$ Å at $T = 150$ K for BFA and $a = 3.933(1)$ Å and $c = 12.254(3)$ Å at $T = 165$ K for SFCA. The strain distribution along c, determined from the width of the $(00l)$ Bragg reflections, is $\Delta c/c = 0.08$ % and 0.25 % for BFA and SFCA, respectively. The detailed thermo-magnetic histories for the x-ray diffraction measurements on both samples are given in the Appendix.

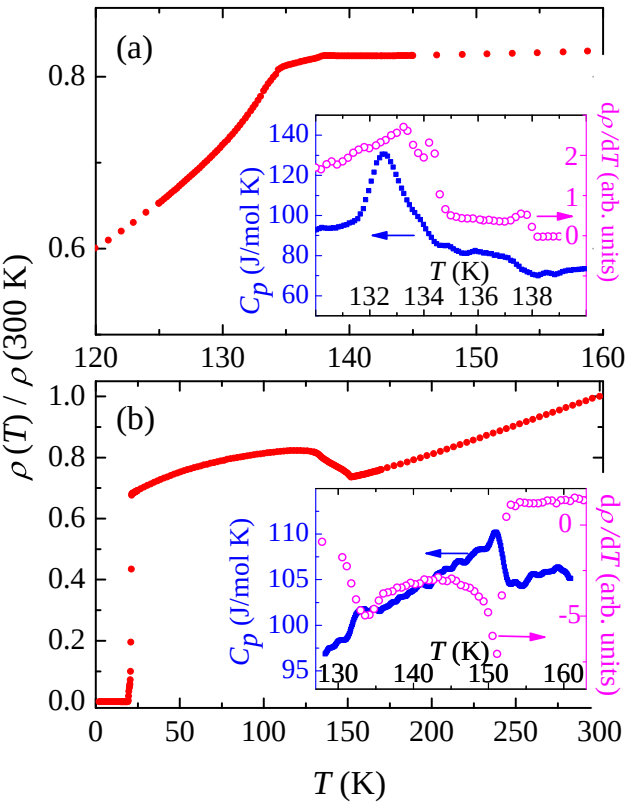

FIG. 1: In-plane resistivity curves at $B = 0$ T for the $BaFe_2As_2$ (BFA) (a) and $Sr(Fe_{1-x}Co_x)_2As_2$ (SFCA) (b) samples investigated in this work. The insets show the specific heat C_p and the resistivity slope in a reduced temperature interval.

III. RESULTS AND ANALYSIS

A. Specific heat and resistivity

Figures 1(a,b) show in-plane resistivity (ρ) curves for BFA and SFCA, respectively. The insets show the specific heat (C_p) and resistivity slope (dρ/dT) in narrow T intervals. For BFA, a relatively strong peak in C_p is observed at $T_{AF}^{BFA} = 132.5$ K with a weaker step-like component at $T_o^{BFA} = 137$ K, which mark the bulk AFM transition and onset of the orthorhombic phase, respectively. We did not observe latent heat at T_{AF} or T_o in either samples[30]. The dρ/dT curve shows a close correspondence with C_p, again indicating two separated transitions. The resistivity of BFA shows a steady drop below $\sim T_{AF}$, which is characteristic of this material. The separation between T_{AF} and T_o for our BFA sam-

ple is substantially larger than that reported for crystals grown by the self-flux method[12,31]. For SFCA, besides the superconducting transition at $T_c = 22$ K, well separated magnetic and nematic/structural bulk transitions are identified in both resistivity and specific heat experiments, with $T_{AF}^{SFCA} = 132$ K and $T_o^{SFCA} = 152$ K.

B. X-ray diffraction

The structural transition of BFA was investigated by reciprocal-space (h h l=12) scans around $h = 2$. Figure 2(a) shows a contour plot of such scans as a function of T, with $B = 0$ T. The reciprocal space indexing was defined with respect to the tetragonal cell lattice parameters at $T = 150$ K. For $T > T_o$, a single tetragonal phase is realized, while for $T_{AF} < T < T_o$ orthorhombic (4 0 12) and (0 4 12) reflections are observed simultaneously with the tetragonal (2 2 12) peak. Below T_{AF}, only orthorhombic reflections are observed. This result indicates that the tetragonal phase is entirely eliminated in the magnetically ordered state, while a coexistence of tetragonal and orthorhombic domains takes place in the T interval between T_{AF} and T_o. We did not observe coexistence of orthorhombic phases with distinct lattice parameters in our sample at any temperature[12]. For $B = 5.9$ T, the temperature associated with the onset of the tetragonal phase is decreased by ~ 1 K with respect to zero field [see Fig. 2(b)], while T_o is field-independent.

Additional insight into the dependence of the crystal structure of BFA on the magnetic field is gained by (h h l=12) scans as a function of field at a fixed $T = 135$ K, i.e., between T_{AF} and T_o [see Fig. 2(c)]. For this specific measurement, special care was taken to realign the sample/diffractometer set at this reflection for each field value, correcting from small movements of the experimental setup and thus retrieving meaningful quantitative information on the B-dependence of the investigated Bragg reflection intensities. An increasing field reduces the relative area of the (4 0 12) and (0 4 12) orthorhombic reflections with respect to the (2 2 12) tetragonal peak, indicating that the field promotes a colonization of the orthorhombic domains by the tetragonal ones in the nematic phase. No significant change in the relative intensities of the (4 0 12) and (0 4 12) orthorhombic reflections is noticed under applied field at this temperature, indicating that relevant detwinning may be achievable only at higher fields[32].

In order to extend our investigation to a compound with similar T_{AF} but with largely separated magnetic and structural transitions, the temperature and magnetic field dependencies of the crystal lattice of SFCA were also probed. Figures 3(a) and 3(b) show contour plots of (h h l=20) reciprocal space scans around $h = 2$ between $T = 110$ and 161 K, with $B = 0$ T and $B = 3.5$ T, respectively. Figures 3(c-h) show the detailed (h h l=20) scans at selected temperatures. Here, the reciprocal space indexing was defined with respect to the tetragonal cell at

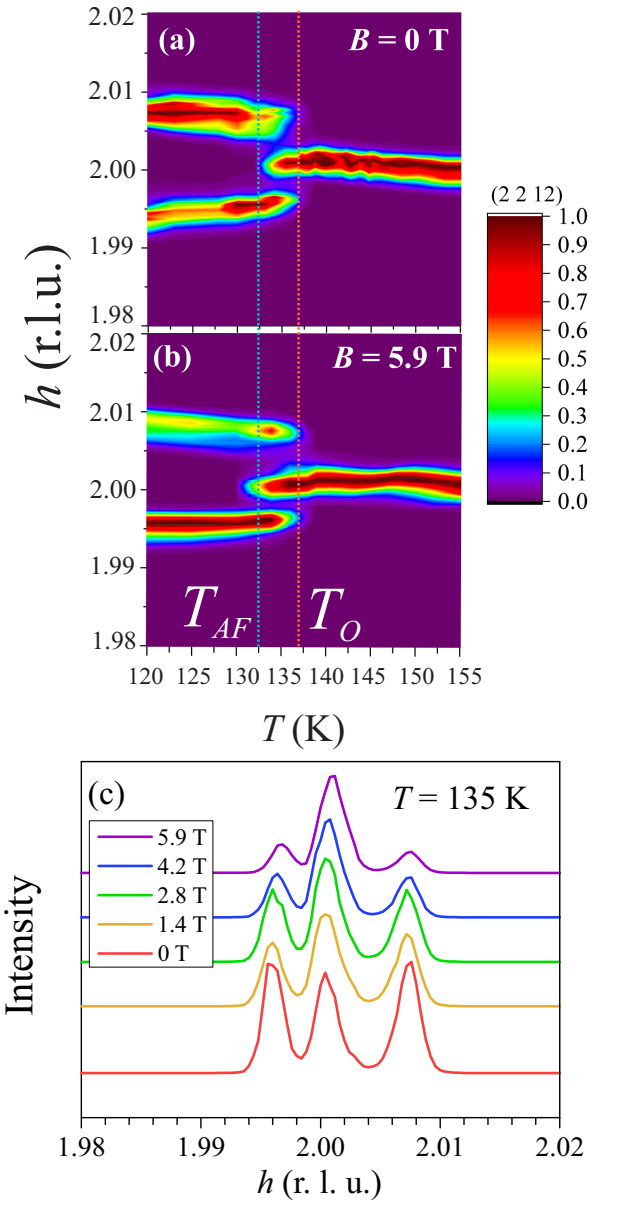

FIG. 2: Contour plots of the x-ray scattering of BFA around the (h h 12) reflection (tetragonal axes), at zero field (a) and $B = 5.9$ T (b), where "r.l.u." is a shorthand for reciprocal lattice units. The transition temperatures T_{AF} and T_o at zero field are indicated as vertical lines [see also Fig. 1(a)]. (c) (h h 12) scans (tetragonal axes) of BFA at $T = 135$ K as a function of the applied magnetic field.

$T = 161$ K. Contrary to BFA, where the excellent crystal quality led to rather sharp peaks in reciprocal-space scans, the Bragg reflections of SFCA are much broader and do not present a single peak shape even in the tetragonal phase. This is presumably due to microscopic fluctuations of the Co-content along the crystal, which lead to fluctuations of lattice parameters and a consequent blurring of the reciprocal-space scans. This effect seriously limits our capacity to investigate in detail the lattice pa-

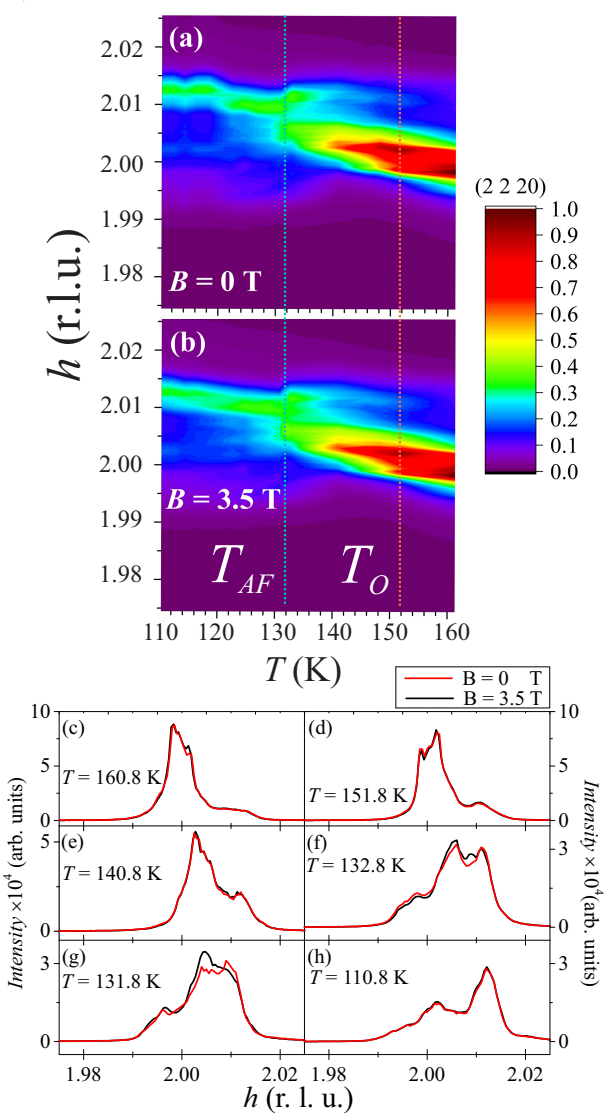

FIG. 3: Contour plots of the x-ray scattering of SFCA around the (h h 20) reflection (tetragonal axes), at zero field (a) and $B = 3.49$ T (b). The transition temperatures T_{AF} and T_o are indicated as vertical lines [see also Fig. 1(b)]. In the color scale, the intensities were divided by a global factor of 9×10^4 counts. (c-h) Unnormalized (h h 20) scans (tetragonal axes) of SFCA at selected temperatures for $B = 0$ T and $B = 3.49$ T.

rameters changes of SCFA as a function of temperature and magnetic field. Nonetheless, it is still possible to see relevant changes in the crystal structure in the studied temperature interval, which seem to be associated with the transitions at T_{AF} and T_o [see Fig. 3(a)]. At 110.8 K, it is possible to identify two separated maxima that we ascribe to the orthorhombic (4 0 20) and (0 4 20) reflections [see Fig. 3(h)], while the diffracted intensities at 160.8 K are associated with the (2 2 20) reflection of a pure tetragonal phase [see Fig. 3(c)]. At intermediate temperatures, a more complex scattering signal is observed, which is presumably associated with a coexistence of tetragonal and orthorhombic domains such as in BFA. It is interesting to note that the scans at 131.8 K and 132.8 K, i.e., near T_{AF}, show a marked B-dependence, with a central peak likely associated with the tetragonal domains being favored by the application of field [see Figs. 3(f,g)]. Overall, our results in SCFA support the conclusion that magnetic fields favor the tetragonal structure in the vicinity of T_{AF}.

IV. DISCUSSION

Considering the distinct and well defined transition temperatures revealed by specific heat measurements and the sharp features observed by resistivity at T_{AF} and T_o, it is evident that two separate bulk phase transitions occur for both investigated samples, dismissing the alternative scenario where one would have a single, broad phase transition occurring between T_{AF} and T_o. Also, the temperature dependence of the x-ray profiles for BFA shown in Fig. 2(a,b) confirms that T_o marks the appearance of an orthorhombic phase that coexists with the tetragonal phase down to T_{AF}. The changes in the equilibrium between the orthorhombic and tetragonal domains are rather abrupt at both T_{AF} and T_o, arguing again in favor of two sharp phase transitions at these temperatures rather than a single broadened phase transition. The x-ray data for SFCA are less clear than for BFA [see Fig. 3(a,b)] due to the lattice strain fluctuations caused by Co substitution. Still, relatively abrupt structural changes are also observed for SFCA at T_{AF}, while a more continuous evolution is noticed between T_{AF} and T_o.

The coexistence of orthorhombic and tetragonal domains between T_{AF} and T_o observed for BFA reveals that the probed crystal is structurally inhomogeneous in this temperature interval. Thus, the sample volume sampled by the x-rays is separated into domains where the structural phase transition coincides with the magnetic phase transition at T_{AF}, and domains where the structural phase transition occurs at a distinct temperature $T_o > T_{AF}$. It is thus safe to state that the orthorhombic phase can be nucleated at T_o slightly above T_{AF}, however such nucleation is extremely delicate leading to phase separation even for undoped crystals of BFA. Below T_{AF}, a stable and homogeneous orthorhombic phase takes over, with no sign of tetragonal domains.

It is in such scenario of a delicate balance between orthogonal and tetragonal domains that our x-ray diffraction data under applied magnetic field must be interpreted. First of all, the temperature where the tetragonal domains disappear for BFA is shown to be reduced under an applied field of 5.9 T (see above). Since this temperature coincides with T_{AF} at zero field, our result may be interpreted in terms of a slight B-dependence of T_{AF}. A slight reduction of T_{AF} with field is not surprising, since the external field also contributes to the magnetic Hamiltonian. Although such magnetic dipolar

term is arguably small compared to exchange, it may be sufficiently large to shift T_{AF} by a significant amount. It is also interesting to note that no significant variation of T_o is observed with B, suggesting a smaller influence of the field-induced magnetic dipolar interaction in the definition of T_o than for T_{AF}.

An insightful result is the field-induced enhancement of the tetragonal domains at $T = 135$ K for BFA, which is an intermediate temperature between T_{AF} and T_o [see Fig. 2(c)]. This indicates that even in the non-magnetic state ($T > T_{AF}$), the fine balance between the tetragonal and orthorhombic domains can be tuned by a magnetic dipolar interaction. This experimental observation provides strong experimental evidence for a magnetically driven structural transition even for the domains with $T_o > T_{AF}$. In a broader perspective, it favors magnetism as the dominant player driving the structural and nematic phase transitions in Fe pnictides. Notice that, in the alternative charge/orbital scenario where a primary orbital ordering transition at T_o would drive the magnetic transition at T_{AF}, the orthorhombic phase at $T_{AF} < T < T_o$ is not rooted in or coupled with magnetism, and therefore there would be no clear microscopic mechanism for the observed enhancement of the tetragonal domains with increasing magnetic fields in this temperature region.

For SFCA, the blurring of the Bragg reflections associated with fluctuations in the Co content prevents a detailed analysis of the magnetic field dependence of the balance between tetragonal and orthorhombic domains. Still, from the data shown in Figs. 3(c-h) it can be safely stated that the most appreciable crystal structure sensitivity of this compound to an external magnetic field is found at the vicinity of T_{AF}, such as in BFA.

We finally consider the relative insensitivity of the crystal structure to magnetic fields at temperatures far above T_{AF} for both BFA and SFCA. Particularly, the onset temperature of the orthorhombic phase (T_o) is insensitive to magnetic fields up to 5.9 T in BFA [see Figs. 2(a) and 2(b)]. This fact might appear to be at odds with our conclusion above that magnetism is the driver of the structural transition at T_o. Notheless, it is worth noting that the dipolar coupling of Fe moments with an external magnetic field of a few tesla is a relatively weak interaction compared to magnetic exchange terms in these materials, thus the effect of B in the tetragonal/ortorhombic phase competition is expected to become most discernible only at magnetic criticality, i.e., at the vicinity of T_{AF} where even small perturbations to the magnetic Hamiltonian may produce an observable effect. Instead, at $T_o > T_{AF}$, the spin fluctuations are non-critical, and therefore the possible influence of the magnetic field on T_o may fall below our observation limit.

V. CONCLUSIONS

In summary, the B-dependence of the tetragonal-orthorhombic transition in representative members of the 122 family of FeSCs indicate that the magnetic field favors the tetragonal phase against the orthorhombic one at the close vicinity of T_{AF}, while no significant effect of the magnetic field on the orthorhombic onset temperature T_o is observed. These observations place important constraints on the possible interplay between the structural, nematic and magnetic transitions in Fe pnictides, favoring magnetism as the primary driver of the structural transition at $T_o > T_{AF}$.

Appendix A: Thermo-magnetic history for x-ray diffraction measurements

The temperature stability during each x-ray diffraction scan was better than 0.1 K for all experiments. The x-ray diffraction data for the (2 2 12) reflection (tetragonal cell) of BFA presented in Fig. 2(a) ($B = 0$ T) were acquired in the following sequence of temperatures (K): 153.3, 150.4, 148.4, 146.3, 145.3, 144.8, 144.3, 143.8, 143.2, 142.7, 142.2, 141.7, 141.2, 140.7, 139.7, 139.2, 138.7, 138.2, 137.7, 137.2, 136.2, 134.1, 132.1, 128.1, 123.0. The diffraction data with $B = 5.9$ T [Fig. 1(b)] was acquired in the following sequence of temperatures (K): 154.9, 151.9, 149.9, 147.8, 146.8, 146.3, 145.8, 145.3, 144.8, 144.3, 143.8, 143.3, 142.8, 142.3, 141.3, 140.8, 140.3, 139.8, 139.3, 138.8, 137.8, 135.8, 133.8, 129.8, 124.8, 119.8. Special care was taken to avoid overcooling during temperature changes. For these measurements, a single alignment was performed at the highest temperature for each field to optimize the reflection intensity, i.e., intermediate realignments at each temperature were not performed. A normalization to the maximum intensity of each h-scan was performed to produce the contour plots of Figs. 2(a) and 2(b). This normalization procedure is not critical to the conclusions of this work.

The (2 2 12) reflection of $BaFe_2As_2$ was also probed at fixed temperature $T = 135$ K as a function of magnetic field, as shown in Fig. 2(c). In this case, the magnetic field was increased from 0 to 5.9 T, where for each field the sample and diffractometer were realigned to maximize the intensity of the tetragonal peak. This procedure was necessary due to small movements of the experimental setup that occurred at each field change as a result of significant stray magnetic fields. In this case, no normalization was performed to display the data of Fig. 2(c).

The x-ray diffraction measurements for the (2 2 20) reflection (tetragonal cell) of SFCA were performed in the following sequence of temperatures (magnetic fields): 160.8 K (3.5 T), 160.8 K (0 T), 151.7 K (0 T), 151.7 K (3.5 T), 147.9 K (3.5 T), 147.9 K (0 T), 145.5 K (0 T), 145.5 K (3.5 T), 140.8 K (3.5 T), 140.8 K (0 T), 132.8 K (0 T), 132.8 K (3.5 T), 131.8 K (3.5 T), 131.8 K (0 T), 124.6 K (3.5 T), 124.6 K (0 T), 114.6 K (0 T), 114.6 K

(3.5 T), 110.8 K (3.5 T), 110.8 K (0 T), with realignments being performed at each field change. The data of Figs. 3(c-h) are shown without any normalization procedure, while the false color intensity scale of the plots of Figs. 3(a) and 3(b) was divided by a global factor for clarity.

Acknowledgments

We thank M.A. Eleotério for assistance in conducting the x-ray diffraction experiments. LNLS is acknowledged for concession of beamtime. This work was supported by FAPESP Grants 2012/04870-7, 2012/05906-3, and 2015/15665-3, and CNPq, Brazil.

[1] Kamihara, T. Watanabe, M. Hirano, and H. Hosono, J. Am. Chem. Soc. **130**, 3296 (2008).
[2] J. Paglione and R.L. Greene, Nature Phys. **6** 645 (2010).
[3] R.M. Fernandes and J. Schmalian, Supercond. Sci. Technol. **25**, 084005 (2012).
[4] R.M. Fernandes, A.V. Chubukov, and J. Schmalian, Nature Phys. **10**, 97 (2014).
[5] J.-F. Ge, Z.-L. Liu, C. Liu, C.-L. Gao, D. Qian, Q.-K. Xue, Y. Liu and J.-F. Jia, Nature Mater. **14**, 285 (2015).
[6] J.-H. Chu, J.G. Analytis, K. De Greeve, P.L. McMahon, Z. Islam, Y. Yamamoto, and I.R. Fisher, Science **329**, 824 (2010).
[7] A. Jesche, F. Nitsche, S. Probst, Th. Doert, P. Müller, and M. Ruck, Phys. Rev. B **86**, 134511 (2012).
[8] H.-H. Kuo, J.-H. Chu, J.C. Palmstrom, S.A. Kivelson, and I.R. Fisher, Science **352**, 958 (2016).
[9] N. Ni, S. Nandi, A. Kreyssig, A.I. Goldman, E.D. Mun, S.L. Bud'ko, and P.C. Canfield, Phys. Rev. B **78**, 014523 (2008).
[10] A.I. Goldman, D.N. Argyriou, B. Ouladdiaf, T. Chatterji, A. Kreyssig, S. Nandi, N. Ni, S.L. Bud'ko, P.C. Canfield, and R.J. McQueeney, Phys. Rev. B **78**, 100506(R) (2008).
[11] H. Li, W. Tian, J.L. Zarestky, A. Kreyssig, N. Ni, S.L. Bud'ko, P.C. Canfield, A.I. Goldman, R.J. McQueeney, and D. Vaknin, Phys. Rev. B **80**, 054407 (2009).
[12] M.G. Kim, R.M. Fernandes, A. Kreyssig, J.W. kim, A. Thaler, S.L. Bud'ko, P.C. Canfield, R.J. McQueeney, J. Schmalian, and A.I. Goldman, Phys. Rev. B **83**, 134522 (2011).
[13] T.M. Garitezi, C. Adriano, P.F.S. Rosa, E.M. Bittar, L. Bufaical, R.L. de Almeida, E. Granado, T. Grant, Z. Fisk, M.A. Avila, R.A. Ribeiro, P.L. Kuhns, A.P. Reyes, R.R. Urbano, and P.G. Pagliuso, Braz. J. Phys. **43**, 223 (2013).
[14] M. Radaelli, Master Thesis, "Gleb Wataghin" Institute of Physics, University of Campinas (2017).
[15] M.A. McGuire, A.D. Christianson, A.S. Sefat, B.C. Sales, M.D. Lumsden, R. Jin E.A. Payzant, D. Mandrus, Y. Luan, V. Keppens, V. Varadarajan, J.W. Brill, R.P. Hermann, M.T. Sougrati, F. Grandjean, and G.J. Long, Phys. Rev. B **78**, 094517 (2008).
[16] J.-Q. Yan, S. Nandi, J.L. Zarestky, W. Tian, A. Kreyssig, B. Jensen, A. Kracher, K.W. Dennis, R.J. McQueeney, A.I. Goldman, R.W. McCallum, and T.A. Lograsso, Appl. Phys. Lett. **95**, 222504 (2009).
[17] H.-F. Li, W. Tian, Q.-Q. Yan, J.L. Zarestky, R.W. McCallum, T.A. Lograsso, and D. Vaknin, Phys. Rev. B **82**, 064409 (2010).
[18] D.K. Pratt, W. Tian, A. Dreyssig, J.L. Zarestky, S. Nandi, N. Ni, S.L. Bud'ko, P.C. Canfield, A.I. Goldman, and R.J. McQueeney, Phys. Rev. Lett. **103**, 087001 (2009).
[19] M.M. Piva, M. Besser, K. Mydeen, T.M. Garitezi, P.F.S. Rosa, C. Adriano, T. Grant, Z. Fisk, R.R. Urbano, M. Nicklas, and P.G. Pagliuso, J. Phys.: Condens. Matter **27**, 145701 (2015).
[20] T.M. McQueen, A.J. Williams, P.W. Stephens, J. Tao, Y. Zhu, V. Ksenofontov, F. Casper, C. Felser, and R.J. Cava, Phys. Rev. Lett. **103**, 057002 (2009).
[21] S.-H. Baek, D.V. Efremov, J.M. Ok, J.S. Kim, J. van den Brink, and B. Büchner, Nature Mater. **14**, 210 (2014).
[22] A.E. Böhmer, T. Arai, F. Hardy, T. Hattori, T. Iye, T. Wolf, H. v. Löhneysen, K. Ishida, and C. Meingast, Phys. Rev. Lett. **114**, 027001 (2015).
[23] U.F. Kaneko, P.F. Gomes, A.F. García-Flores, J.-Q. Yan, T.A. Lograsso, G.E. Barberis, D. Vaknin, and E. Granado, Phys. Rev. B **96**, 014506 (2017).
[24] A.V. Chubukov, R.M. Fernandes, and J. Schmalian, Phys. Rev. B **91**, 201105(R) (2015).
[25] P.F.S. Rosa, C. Adriano, T.M. Garitezi, T. Grant, Z. Fisk, R.R. Urbano and P.G. Pagliuso, Sci. Rep. **4**, 6543 (2014) and references therein.
[26] F.A. Lima, M.E. Saleta, R.J.S. Pagliuca, M.A. Eleotério, R.D. Reis, J. Fonseca Júnior, B. Meyer, E.M. Bittar, N.M. Souza-Neto, and E. Granado, J. Synchr. Rad. **23**, 1538 (2016).
[27] A. Leithe-Jasper, W. Schnelle, C. Geibel, and H. Rosner, Phys. Rev. Lett. **101**, 207004 (2008).
[28] J.S. Kim, S. Khim, H.J. Kim, M.J. Eom, J.M. Law, R.K. Kremer, J.H. Shim, and K.H. Kim, Phys. Rev. B **82**, 024510 (2010).
[29] E. Lengyel, M. Kumar, W. Schnelle, A. Leithe-Jasper, and M. Nicklas, Phys. Status Solidi B **254**, 1600154 (2017).
[30] J.C. Lashley *et al.* Cryogenics **43**, 369 (2003).
[31] C.R. Rotundu, B. Freelon, T.R. Forrest, S.D. Wilson, P.N. Valdivia, G. Pinuellas, A. Kim, J.-W. Kim, Z. Islam, E. Bourret-Courchesne, N.E. Phillips, and R.J. Birgeneau, Phys. Rev. B **82**, 144525 (2010).
[32] J.-H. Chu, J.G. Analytis, D. Press, K. De Greeve, T.D. Ladd, Y. Yamamoto, and I.R. Fisher, Phys. Rev. B **81**, 214502 (2010).